Electronic Supplementary Information (ESI) for

Two-component bimetallic sulfides Enhancing OER Activity

Chengjie Liao,[a] Ting Liu,[a] Hui Chang,[a] Yufeng Li,[a] Jin Lu,[a] Dexiang Zhang, *[a] Tian Wen*[ab] and Zhiqiang Jiang*

a. Vanadium and Titanium Critical Strategic Materials Key Laboratory of Sichuan Province, College of Vanadium and Titanium, Panzhihua University, Sichuan, 617000, P. R. China.

b. School of Chemistry, Monash University, Clayton VIC 3800, Australia.

E-mail: jiangzq@pzhu.edu.cn

zhangdexiang @pzhu.edu.cn

tian.wen1@monash.edu

Part I: Experimental Section

1. Characterization of the catalyst

The structural analysis of the catalyst was performed using a (Mo-Kα, λ = 0.71073 Å) X-ray single-crystal diffractometer. Phase composition and crystallinity were characterized by powder X-ray diffraction (PXRD) with a Dongfang Ovoid DX-2007 instrument. Morphological and structural features were examined using a FEI Inspect F50 scanning electron microscope (SEM) and a JEOL JEM-2100 LaB6 transmission electron microscope (TEM). Fourier transform infrared (FTIR) spectroscopy was conducted on a Bruker VERTEX 70V spectrometer to identify functional groups and obtain infrared spectra. The chemical states and elemental environments were analyzed by X-ray photoelectron spectroscopy (XPS) using a Thermo Fisher Escalab 250 Xi spectrometer.

2. Electrochemical characterization

Electrochemical measurements were carried out using a CHI760E electrochemical workstation (Shanghai Chenhua) in conjunction with a standard three-electrode system at room temperature. The working electrode was a nickel mesh coated with the catalyst, the counter electrode was a platinum sheet, and the reference electrode was Ag/AgCl (with a 3 M KCl salt bridge). Notably, a Hg/HgO reference electrode was employed to assess the intrinsic catalytic activity of the catalysts using a glassy carbon electrode. The electrolyte was N_2-saturated 1 M KOH, which served as the medium for oxygen evolution reaction (OER) activity evaluation. Prior to OER testing, the catalyst was activated by cyclic voltammetry (CV) over a potential range of 0 to 0.8 V (vs. Ag/AgCl) at a scan rate of 50 mV s^{-1} until CV curves showed complete overlap. Subsequently, OER performance was assessed via linear sweep voltammetry (LSV) at a scan rate of 5 mV s^{-1}. Electrochemical impedance spectroscopy (EIS) was performed at an applied potential of 0.5 V vs. Ag/AgCl across a frequency range from 10^6 to 0.02 Hz. To determine the electrochemical active surface area (ECSA), CV measurements were conducted within the potential

window of 1.02 to 1.12 V vs. RHE at scan rates ranging from 10 to 50 mV s^{-1}, and the double-layer capacitance (Cdl) was calculated from the resulting data. Finally, long-term electrochemical stability was evaluated through chronoamperometric testing at a constant potential of 0.5 V vs. Ag/AgCl.

3. Synthesis of PZH-9

In a glass reaction flask, cobalt(II) nitrate hexahydrate (0.0291 g), 5,6-dimethylbenzimidazole (0.0147 g), 1,4-naphthalenedicarboxylic acid (0.0216 g), tetramethylammonium bromide (0.0200 g), and ethylene urea (0.0200 g) were accurately weighed and added. Subsequently, N,N-dimethylformamide (0.5 mL), N,N-dimethylacetamide (0.5 mL), and deionized water (0.5 mL) were added sequentially. The resulting mixture was subjected to ultrasonic dissolution for 30 min to ensure homogeneity, followed by transfer to an oven maintained at 120 °C for solvothermal reaction over 48 hours. Upon completion, the reaction vessel was removed and allowed to cool to room temperature naturally. The resulting solid product was collected by centrifugation, washed alternately three times with ethanol and deionized water, and finally dried under ambient conditions to yield purple-black, block-shaped crystals.

4. Synthesis of $Fe_{0.8}Co_{0.2}S$@$FeCoS_2$

0.4039 g of $Fe(NO_3)_3·6H_2O$ was dissolved in 2 mL of anhydrous ethanol to prepare a $Fe(NO_3)_3·6H_2O$ ethanol solution. A suitable amount of PZH-9 was immersed in this solution at room temperature for 24 h. After filtration and drying, Fe@PZH-9 was obtained. Subsequently, 0.030 g of Fe@PZH-9 was evenly spread on one end of a quartz boat, while 0.45 g of sulfur powder was accurately weighed and placed on the opposite end, ensuring that the sulfur was positioned upstream in the gas flow. The quartz boat was then placed in the center of a tube furnace. The temperature was increased to 700 °C at a heating rate of 5 °C/min, followed by a 6-hour annealing process under a continuous flow of inert argon gas. After completion of the thermal

treatment and natural cooling to room temperature, the final product, $Fe_{0.8}Co_{0.2}S@FeCoS_2$, was collected.

5. Synthesis of Compound PZH-9-S

PZH-9 was used without any pre-treatment and directly subjected to high-temperature sulfurization at 700 °C under an inert atmosphere to yield the target catalyst, PZH-9-S.

6. Preparation of OER electrodes

Separately take 30 mg of the prepared catalyst and grind it in an agate mortar for 1 hour. Then, weigh out 10 mg of the ground sample and transfer it to a 1.5 mL centrifuge tube. Add 350 μL of ultrapure water, 100 μL of anhydrous ethanol, and 50 μL of 5 wt.% Nafion solution, followed by ultrasonication for 30 min in an ultrasonic cleaner to obtain a uniformly dispersed ink solution for subsequent use. Using a micropipette, deposit 20 μL of the ink solution twice onto both sides of an L-shaped nickel foam substrate (0.5 × 1 cm^2), achieving a total catalyst loading of 1.6 mg cm^{-2}. After air-drying at room temperature, the resulting electrodes using different catalysts ($Fe_{0.8}Co_{0.2}S@FeCoS_2$, PZH-9-S/NF, RuO_2,) were used as OER working electrodes. A bare NF electrode without any catalyst coating.

Part II: Supplementary Results

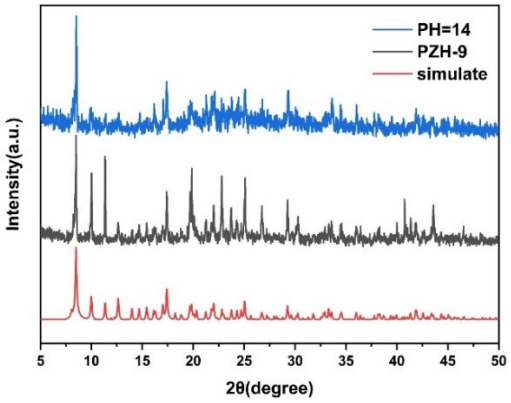

Figure S1. PXRD patterns of the as-synthesized PZH-9 and after immersion in a strongly alkaline environment.

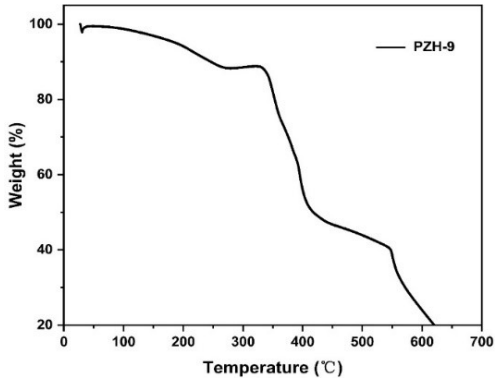

Figure S2. TGA patterns of the as-synthesized PZH-9.

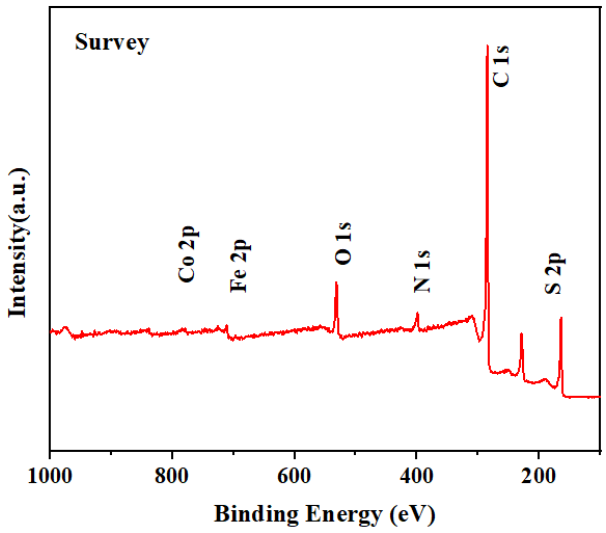

Figure S3. Full survey XPS spectrum of $Fe_{0.8}Co_{0.2}S@FeCoS_2$.

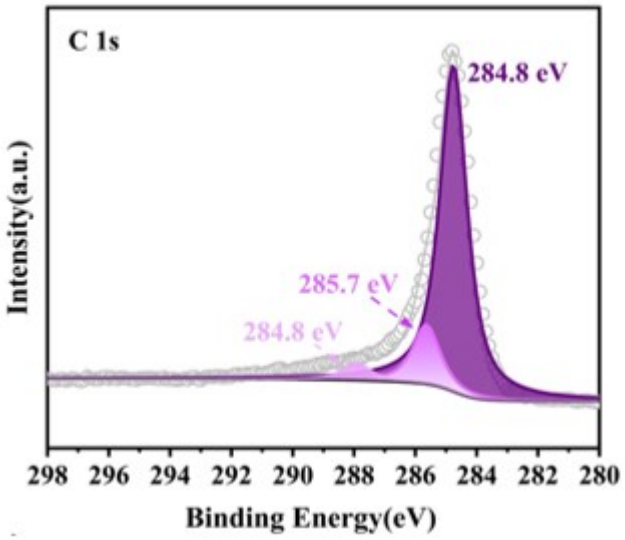

Figure S4. High-resolution C 1s XPS spectrum.

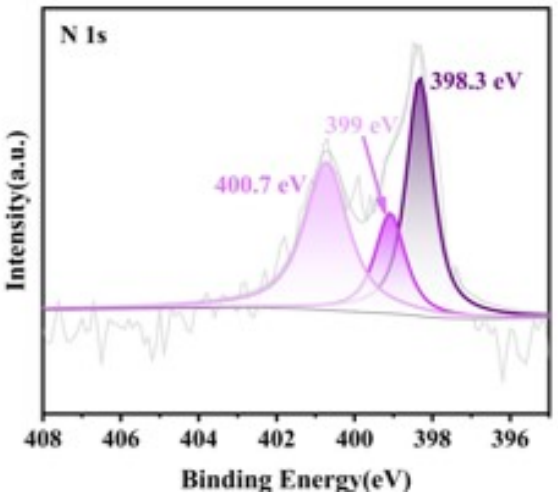

Figure S5. High-resolution N1s XPS spectrum.

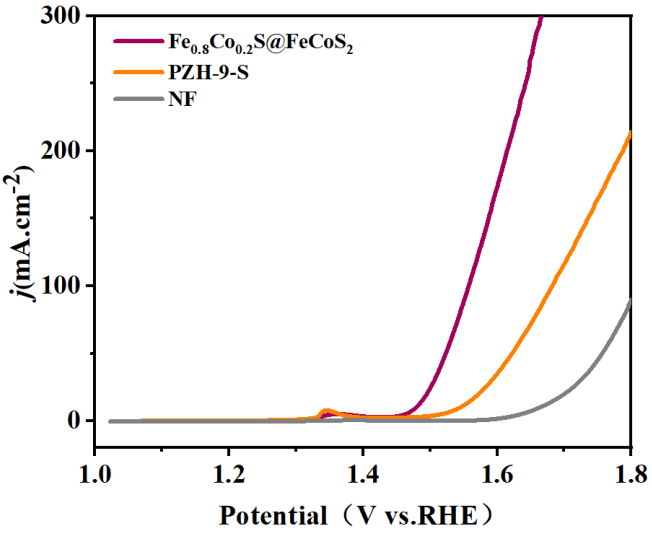

Figure S6. LSV curve of catalysts.

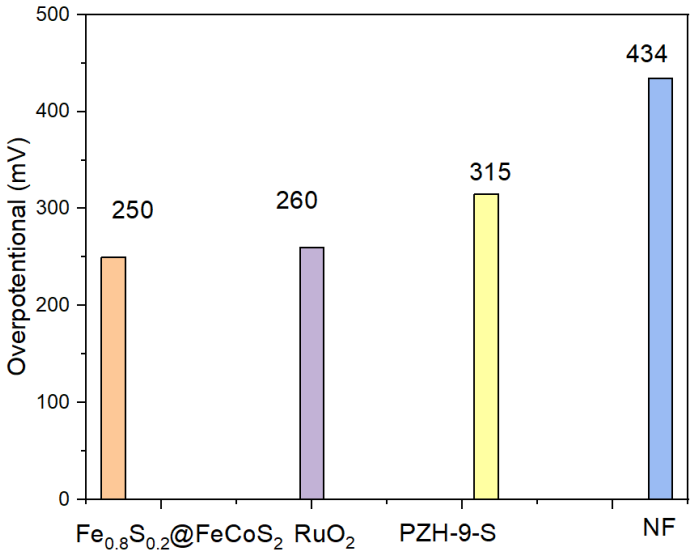

Figure S7. Overpotential of the catalysts.

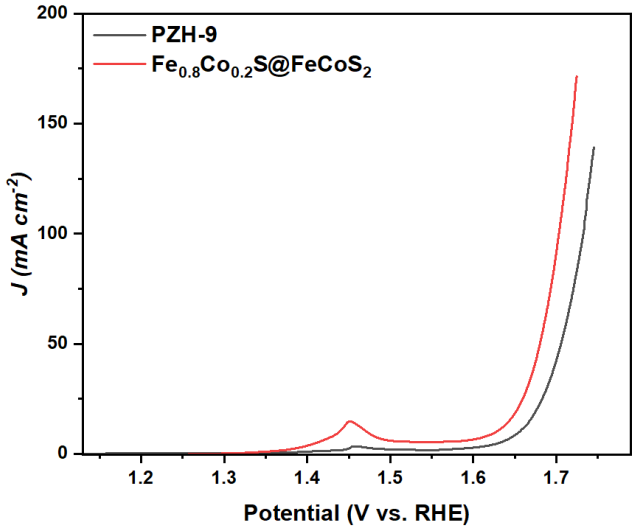

Figure S8. LSV curve of the PZH-9 and $Fe_{0.8}Co_{0.2}S@FeCoS_2$ catalysts, recorded using a Hg/HgO reference electrode.

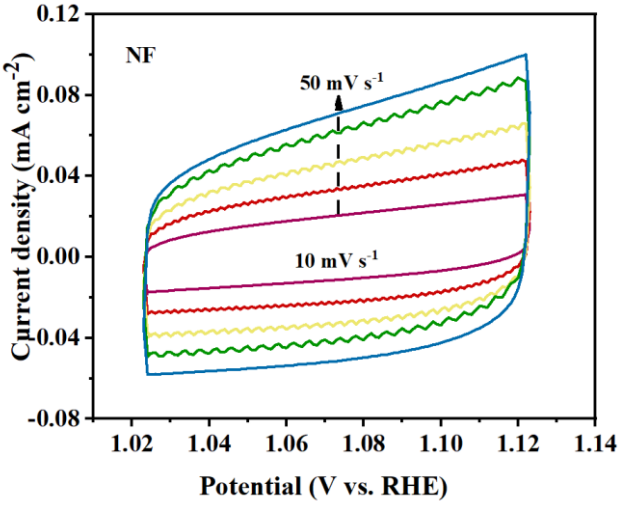

Figure S9. Cyclic voltammetry (CV) curve of nickel foam (NF)

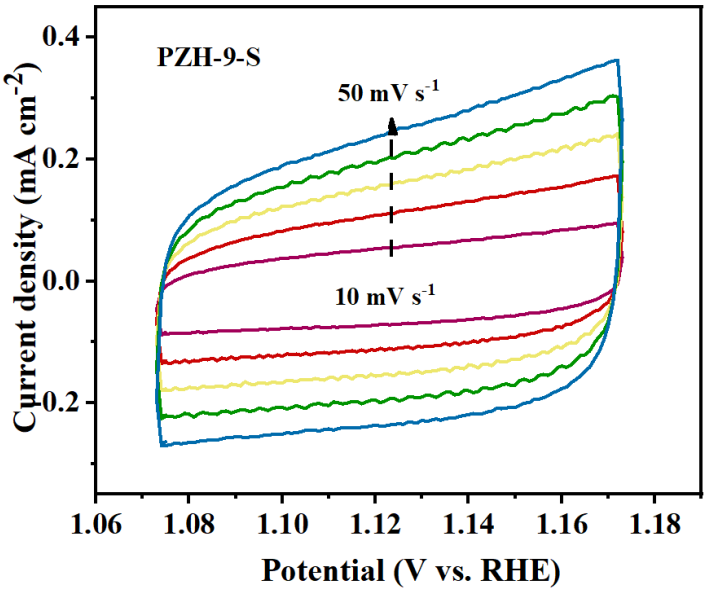

Figure S10. CV curve of PZH-9-S.

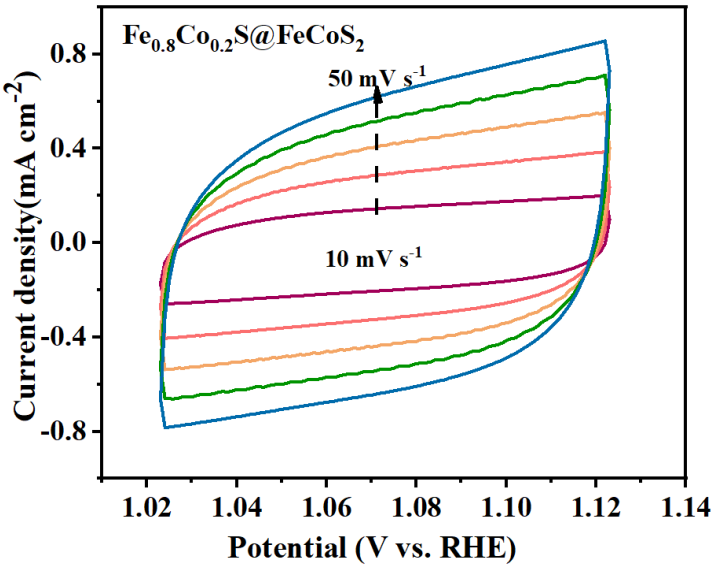

Figure S11. CV of $Fe_{0.8}Co_{0.2}S@FeCoS_2$.

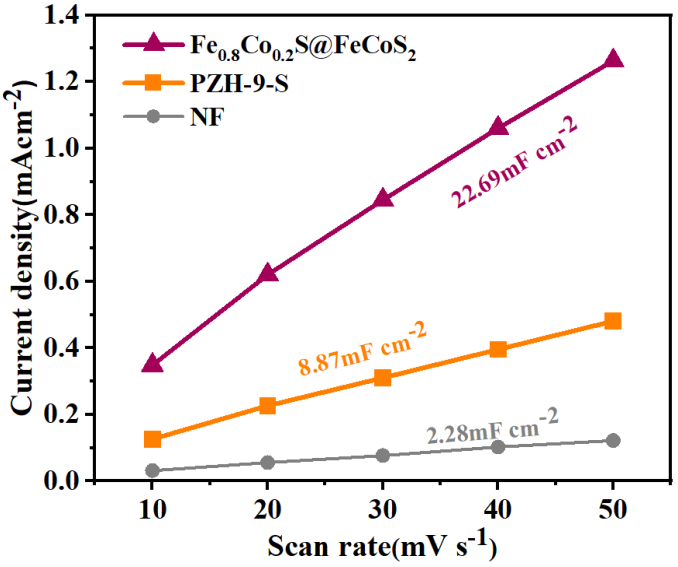

Figure S12. Double-layer capacitance (C_{dl}) of the catalysts.

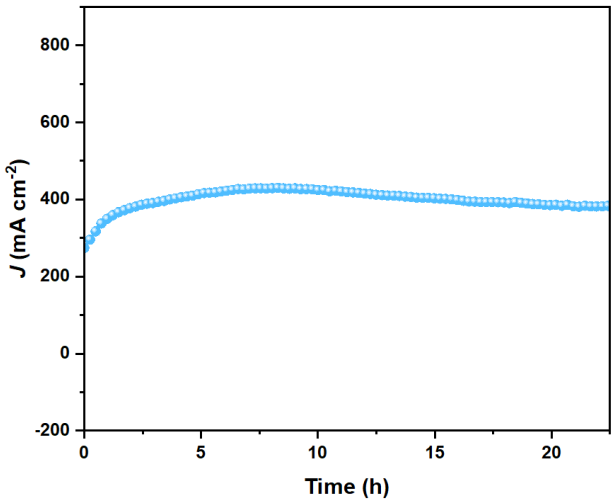

Figure S13. Chronoamperometric i-t curve of the catalyst, showing an overpotential of 1.8 V vs. RHE.

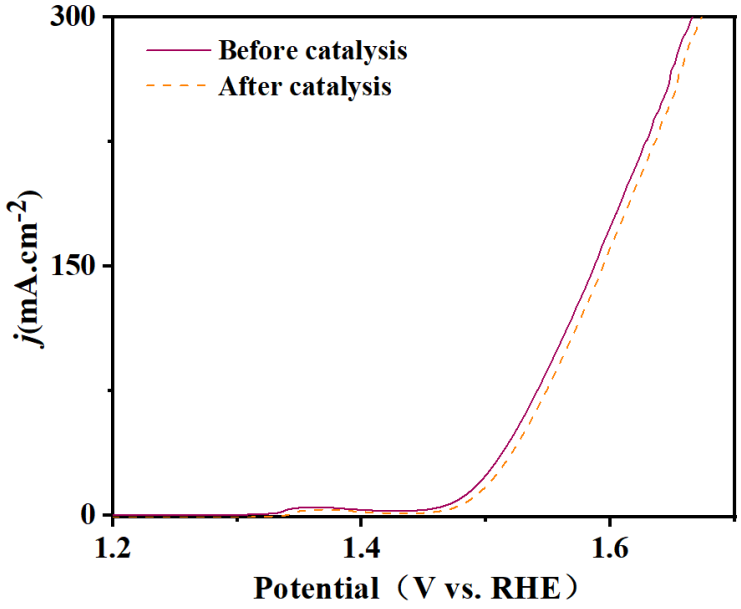

Figure S14. LSV curves of the catalyst before and after stability testing.

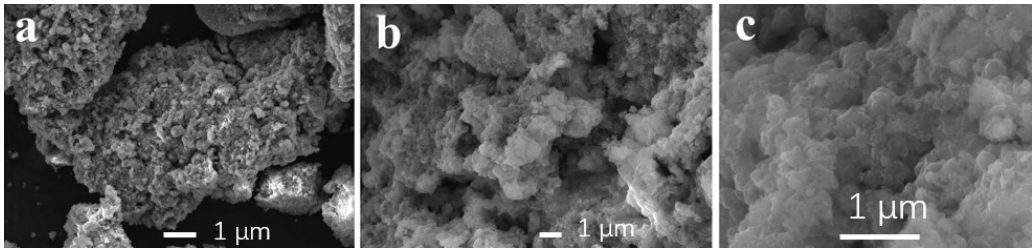

Figure S15. SEM images after stability test.

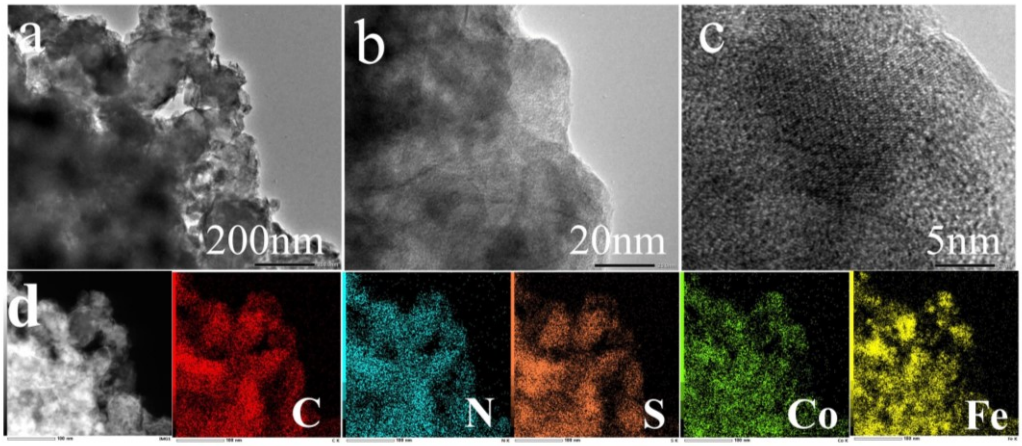

Figure S16. TEM images and elemental mapping after stability testing.

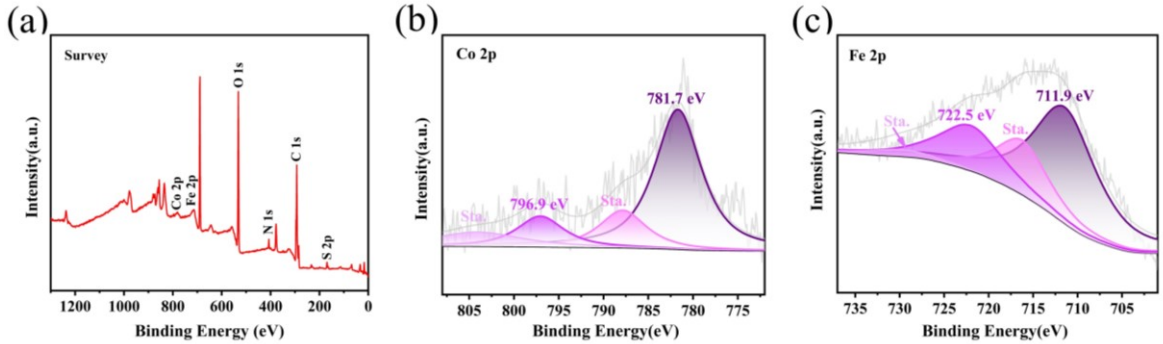

Figure S17. XPS characterization after catalysis. (a) Survey XPS spectrum of $Fe_{0.8}Co_{0.2}S$@$FeCoS_2$. (b) High-resolution XPS spectrum of Co 2p. (c) High-resolution XPS spectrum of Fe 2p.

Table S1. Comparison of the overpotentials of this work with those of other electrocatalysts.

Number	Catalyst	Electrolyte	Overpotential (mV) at 10 mA cm^{-2}	Ref.
1	$Fe_{0.8}Co_{0.2}S$@$FeCoS_2$	1 M KOH	**250**	**This work**
2	CoFeBTC MOF	1 M KOH	310	[1]
3	CoNi-MOF	1 M KOH	350	[2]
4	Co-MOF	1 M KOH	420	
5	$Ni_{10}Fe$-BTC	1 M KOH	346	[3]
6	$Ni_{10}Co$-BTC	1 M KOH	378	
7	COF-C_4N/THQ-Co_2Fe_1	1 M KOH	314	[4]
8	Co-MOF-1	1 M KOH	294	[5]
9	Co-MOF-2	1 M KOH	343	
10	$Co_{2.25}Fe_{0.75}O_4$	1 M KOH	350	[6]
11	HEA-FeMnCuCo	1 M KOH	226	[7]
12	M1S1	1 M KOH	300	[8]
13	CoP/CoP@NPGC-1	1 M KOH	340	[9]
14	CoMo-MI-600	1 M KOH	316	[10]
15	$A_{2.5}$B-CoNi MOFs	1 M KOH	300	[11]

References

[1] Burud M, Patil S A, Jadhav V, et al. Synergistic effect of CoFe bimetallic MOF for efficient electrocatalytic OER in alkaline media[J/OL]. Energy & Fuels, 2025: acs.energyfuels.5c01134. DOI:10.1021/acs.energyfuels.5c01134.

[2] Konavarapu S K, Kim G, Shin K, et al. Boosting electrocatalytic activity of bimetallic CoNi-MOF for OER and HER through a synergistic bimetallic approach[J]. Chemistry – A European Journal, 2025, 31(24): e202500010.

[3] Sondermann L, Jiang W, Shviro M, et al. Nickel-based metal-organic frameworks as electrocatalysts for the oxygen evolution reaction (OER)[J]. Molecules, 2022, 27(4): 1241.

[4] Liu Y, Yang Z D, Zhang R, et al. Highly conjugated 2D COF/MOF composites for bifunctional electrocatalytic alkaline HER and OER with enhanced activity and stability[J/OL]. Industrial Chemistry & Materials, 2026: 10.1039.D5IM00302D. DOI:10.1039/D5IM00302D.
[5] Muthukumar P, Arunkumar G, Pannipara M, et al. Enhancing the electrocatalytic OER activity of co-MOFs through labile solvents coordination[J]. New Journal of Chemistry, 2023, 47(45): 20831-20837.
[6] Saddeler S, Bendt G, Salamon S, et al. Influence of the cobalt content in cobalt iron oxides on the electrocatalytic OER activity[J]. Journal of Materials Chemistry A, 2021, 9(45): 25381-25390.
[7] Bian H, Wang C, Zhao S, et al. Preparation of highly efficient high-entropy alloy catalysts with electrodeposition and corrosion engineering for OER electrocatalysis[J]. International Journal of Hydrogen Energy, 2024, 57: 651-659.
[8] Chen B, Hu P, Yang F, et al. In situ porousized MoS_2 nano islands enhance HER/OER bifunctional electrocatalysis[J]. Small, 2023, 19(14): 2207177.
[9] Gong W, Zhang H, Yang L, et al. Core@shell MOFs derived Co2P/CoP@NPGC as a highly-active bifunctional electrocatalyst for ORR/OER[J]. Journal of Industrial and Engineering Chemistry, 2022, 106: 492-502.
[10] Guo Y, Huang Q, Ding J, et al. CoMo carbide/nitride from bimetallic MOF precursors for enhanced OER performance[J]. International Journal of Hydrogen Energy, 2021, 46(43): 22268-22276.
[11] Ma L, Xue Q, Dang Y, et al. A novel bimetallic organic framework catalyst induced by dual-ligand for highly efficient oxygen evolution[J]. Journal of Colloid and Interface Science, 2024, 655: 234-242.

Table S1. Summary of Crystalographic Data and Refinement Results

Compound	PZH-9
Formula	$C_{42}H_{43}N_4O_{12}Co_2$
Mr	419.27
T (K)	293(2)
crystal system	monoclinic
space group	*Cc*
a (Å)	20.1162(4)
b (Å)	14.0082(2)
c (Å)	16.8283(3)
α (º)	90
β (º)	118.353(2)
γ (º)	90
V (Å 3)	4173.21(14)
Z	52
F(000)	2548
*D*calc (g cm^{-3})	1.31
μ (mm^{-1})	39.833
CCDC No.	**2492172**

[a]$R_1 = \Sigma(|Fo| - |Fc|)/\Sigma|Fo|$, $wR_2 = [\Sigma w(Fo^2 - Fc^2)^2/\Sigma w(Fo^2)^2]^{0.5}$